Low Emittance, High Brilliance Relativistic Electron Beams from a Laser-Plasma Accelerator

E. Brunetti, R. P. Shanks, G. G. Manahan, M. R. Islam, B. Ersfeld, M. P. Anania, S. Cipiccia, R. C. Issac, G. Raj, G. Vieux, G. H. Welsh, S. M. Wiggins, and D. A. Jaroszynski*

Physics Department, University of Strathclyde, Glasgow G4 0NG, United Kingdom

(Received 31 August 2010; published 19 November 2010)

Progress in laser wakefield accelerators indicates their suitability as a driver of compact free-electron lasers (FELs). High brightness is defined by the normalized transverse emittance, which should be less than 1π mm mrad for an x-ray FEL. We report high-resolution measurements of the emittance of 125 MeV, monoenergetic beams from a wakefield accelerator. An emittance as low as $1.1 \pm 0.1\pi$ mm mrad is measured using a *pepper-pot* mask. This sets an upper limit on the emittance, which is comparable with conventional linear accelerators. A peak transverse brightness of 5×10^{15} A m^{-1} rad^{-1} makes it suitable for compact XUV FELs.

DOI: 10.1103/PhysRevLett.105.215007 PACS numbers: 52.38.Kd, 41.75.Jv

Synchrotron sources are essential tools for research and technology, because of their spectral range from infrared to x rays [1–4]. They are based on radio-frequency cavities that are limited to accelerating gradients <100 MV/m, which results in large and expensive facilities. This constrains their availability and therefore their impact on research. Plasma has recently been demonstrated as an accelerating medium with gradients 3 orders of magnitude higher than conventional accelerators [5]. Tajima and Dawson in 1979 [6] showed that intense laser pulses can drive plasma density wakes to produce huge electrostatic forces by charge separation that accelerate particles to high energies. Advances in laser technology are making laser wakefield accelerators (LWFAs) a reality, with the demonstration of mm-long 100's MeV [7–9] and cm-long GeV [10] accelerators. Proof-of-principle synchrotron sources driven by LWFAs have been demonstrated in the visible [11] and vacuum ultraviolet [12] ranges. However, free-electron lasers (FELs) and synchrotron sources require high brightness beams. Although the suitability of LWFAs has been indirectly provided by previous studies of the electron energy spread and undulator radiation [13,14], here we present a definite proof by directly measuring the transverse emittance of LWFA beams. The emittance, which is the volume in phase space occupied by the particles, is the main parameter that together with the current defines the brightness and the quality of an accelerator [15]. Beam quality is a measure of the properties of both particle source and beam transport system and directly transfers into the quality of synchrotron and FEL sources, because photon beam brightness and coherence depend on the emittance. The emittance is not a directly observable quantity. It can be found by measuring the beam size at one location while scanning the strength of nearby upstream quadrupoles [16], or by measuring the beam size at several locations, suitably separated in betatron phase, with fixed quadrupoles. The resulting particle spatial and angular distribution can be used to reconstruct the emittance. LWFA generated electrons are, however, best characterized using the pepper-pot method [17–19], which is single shot and not prone to space-charge effects. This technique uses a mask with a grid of holes or slits in dense material to split the beam into small beamlets that drift to a scintillating screen. The measurement of the beamlet positions and sizes yields the beam divergence, which combined with the measurement of the total beam size, gives the emittance. This method has been used for beams up to 508 MeV [20].

In this Letter we present measurements of the emittance of 125 ± 3 MeV (averaged over 200 energy spectra) electron beams from the laser plasma wakefield accelerator on the Advanced Laser-Plasma High-energy Accelerators towards x-rays (ALPHA-X) beam line [21], that have been carried out using the experimental setup shown in Fig. 1. A high-power laser delivers 30 fs, 800 nm, 900 mJ pulses on target. After focusing to a $w_0 = 20$ μm ($1/e^2$ radius) spot by an $f/18$ spherical mirror, a peak intensity of up to 2×10^{18} W cm^{-2} is reached. This corresponds to a normalized vector potential $a_0 = eA/m_e c^2 \approx 1$, where A is the vector potential, c speed of light, and e and m_e electron charge and mass, respectively. The laser beam interacts with a 2 mm diameter supersonic helium gas jet, and

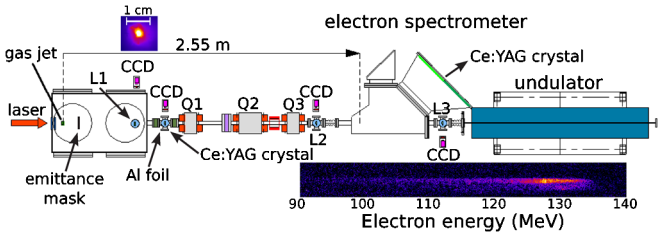

FIG. 1 (color online). Experimental setup. Removable Lanex screens—L1, L2, and L3 and quadrupole magnets—Q1, Q2, and Q3. The distance from the accelerator to the emittance mask is 29.5 cm. Pepper-pot spots are detected on the Ce:YAG crystal 61 cm after the mask. The insets show a typical electron profile on screen L1 and an electron spectrum.

self-compresses to a 10 μm diameter relativistic plasma channel with a density of $n_p = 10^{19}$ cm^{-3}. This type of self-guiding occurs when the laser power exceeds the threshold for relativistic self-focusing $P_{\rm cr} \sim 17\gamma_g^2$ GW [22], where $\gamma_g = 1/\sqrt{1 - v_g^2/c^2} = \omega_0/\omega_p$ is the Lorentz factor associated with v_g, the laser pulse group velocity and ω_0 and $\omega_p = \sqrt{n_p e^2/m_e \epsilon_0}$ are the laser and plasma frequencies, respectively. Relativistic self-focussing increases the field potential and then the ponderomotive force expels charge from the high intensity region, creating an accelerating cavity with a radius $\sqrt{a_0}\lambda_p/\pi$ [23]. During this period the field potential grows from $a_0 = 1$ to $a_0 > 3$, and electrons are self-injected into the cavity, and then accelerated to a maximum energy $\gamma_{\rm max} = 2\gamma_g^2 a_0/3$. Following injection, electrons perform transverse betatron oscillations with an adiabatically changing frequency and amplitude due to the increase in γ. Emittance growth at injection is due to the sudden change of the transverse force, as explained below. In this phase, the transverse emittance increases; afterwards it remains constant.

The design of the emittance measurement system is based on GEANT4 [24] simulations, which show that a mask too thin to completely block 125 MeV electrons still provides accurate emittance measurements. Transmitted electrons are scattered over a wide angle to produce a smooth background, which is removed from the pepper-pot spots by fitting the signal level found between the rows of holes and by applying a Fourier filter. Because of the difficulty of drilling small diameter, high aspect ratio holes in very dense material [20], the efficiency of a thin mask greatly simplifies the measurements. The mask consists of a 125 μm thick tungsten sheet pierced by a 27×27 array of 25 ± 5 μm diameter holes separated by 150 μm, and fixed to a rotation stage 29.5 cm from the gas jet. The beamlets are detected on a 2×2 cm, Ce:YAG crystal placed 61 cm after the mask and imaged by a 14 bit CCD camera, with an overall spatial resolution of 10 μm. A thin Al foil placed in front of the crystal blocks the laser light. Although the destructive nature of the pepper-pot technique does not allow the simultaneous measurement of emittance and electron energy, the good pulse-to-pulse stability of the LWFA allows further diagnostics to be performed under identical conditions after removal of the mask from the beam line.

Figure 2 shows typical pepper-pot emittance spots detected on the Ce:YAG screen. The method described in Ref. [25] is used to evaluate the transverse emittance, defined as the root mean square correlation between the displacement and momentum of the beam particles in the (x, y, x', y') phasespace: $\epsilon_{nx} = \sqrt{\langle \Delta x^2 \rangle \langle \Delta p_x^2 \rangle - \langle \Delta x \Delta p_x \rangle^2}/m_0 c$, with $\Delta x = x - \langle x \rangle$, etc. Emittance values recorded for 64 of 400 consecutive laser shots are presented in Fig. 3. Because of pointing instabilities, beams are emitted within a solid angle of 9×10^{-4} sr. Since the mask subtends 1.5×10^{-4} sr, only $\sim 1/6$th of the shots reach the detection system. The average horizontal emittance (along the laser polarization axis) is $2.2 \pm 0.7\pi$ mm mrad, with a best value of $1.1 \pm 0.1\pi$ mm mrad, which corresponds to the resolution limit of our system. The vertical emittance has an average value of $2.3 \pm 0.6\pi$ mm mrad, and best value of $1.2 \pm 0.1\pi$ mm mrad. Coupled with the observed electron beam divergences of 2–4 mrad, an effective source size smaller than 3 μm is inferred.

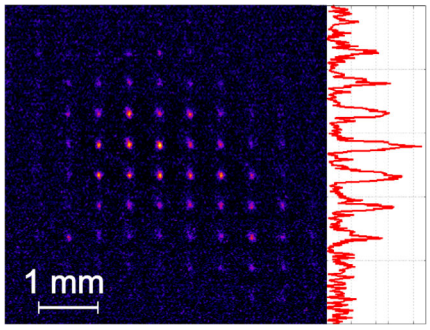

FIG. 2 (color online). A false color, background corrected, pepper-pot image produced on the Ce:YAG crystal by an electron beam after propagation through the emittance mask. A vertical lineout is shown on the right-hand side.

To understand what determines the emittance for our experimental conditions, 2D particle-in-cell (PIC) code OSIRIS [26] simulations have been performed for a 30 fs laser pulse, initially with $a_0 \approx 3$, propagating in plasma with a density of $n_p \approx 10^{19}$ cm^{-3} (Fig. 4). Relativistic self-focussing quickly reduces the initial laser spot w_0 from 20 μm to 10 μm, thus increasing a_0. A slightly higher a_0 in the PIC code simulations compared with experimental values is necessary to enable injection. Figures 4(c)–4(f) show the evolution of the bunch length, σ_z, radius σ_r, energy γ, energy spread σ_γ and σ_γ/γ, and ϵ_{nx} as a function of time for electrons in the (x, p_x) plane (laser polarization plane). The emittance lies between 0.1 and 0.2π mm mrad and the energy spread is of the order of 1% for a relatively short electron bunch length ($\sim$ 1 fs) and 1.4 pC charge. Before electrons are injected at the rear of

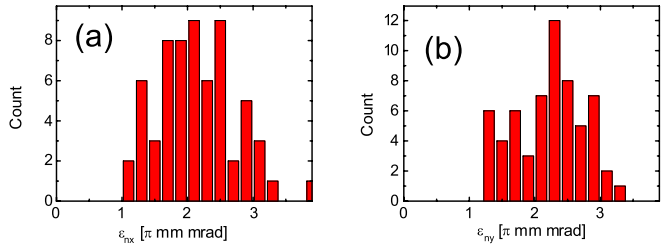

FIG. 3 (color online). Distribution of the horizontal (a) and vertical (b) normalized emittance for a collection of 64 shots. The average values are $\epsilon_{nx} = 2.2 \pm 0.7\pi$ mm mrad and $\epsilon_{ny} = 2.3 \pm 0.6\pi$ mm mrad, respectively.

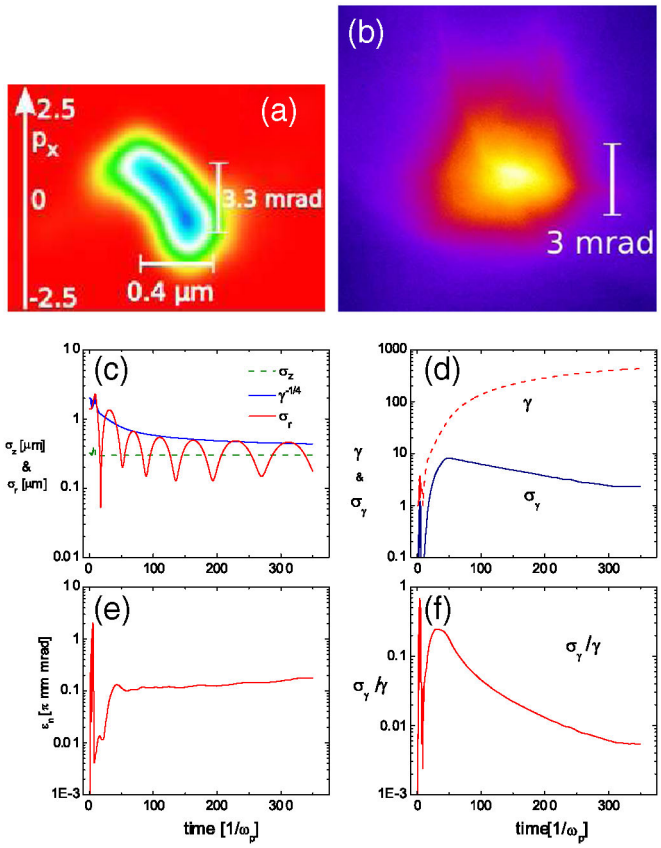

FIG. 4 (color online). (a) 2D PIC simulations showing beam in (x, p_x) space with normalized emittance of 0.1–0.2π mm mrad, FWHM diameter of 0.4 μm and FWHM divergence of 3.3 mrad, (b) image of electron beam profile measured on Ce:YAG crystal, (c)–(f) PIC simulations showing evolution of σ_z, $\gamma^{-1/4}$, σ_r, γ, σ_γ, ϵ_n and σ_γ/γ with time (in units of $1/\omega_p$).

the bubble the emittance is negligible [Fig. 4(e)]. However, at injection, the emittance grows quickly, saturates and then grows again at a much slower rate as electrons reach dephasing. This behavior can be explained by examining the transverse electric and magnetic forces on the electrons (in the comoving frame of reference), due to the ion background (flowing backwards with velocity v_g): $F_x = -m_0\omega_p^2(1 + v_z v_g/c^2)x/2$. While electrons move backwards, with $v_z \approx -c$, the magnetic and electric forces almost cancel, and electrons keep their initial transverse position, x_0, while maintaining a small transverse momentum p_x. The transverse emittance is therefore initially very low. Electrons trapped at the back of the bubble reverse their longitudinal velocity; they then experience the transverse force and start to perform betatron oscillations [27], which are damped at a rate $\gamma^{-1/4}$ as shown in Fig. 4(c). As the particle velocity reverses on a time scale that is short compared with the betatron period, the amplitude is still determined by the initial position x_0, whereas the momentum amplitude and thus the emittance grows with the transverse force, proportional to $(1 + v_z v_g/c^2)$. When $v_z \approx c$, the emittance reaches a saturation value $\epsilon_{nx} = x_0^2 k_p \gamma_g^{1/2} 8^{-1/2}$ just after trapping $\gamma \approx \gamma_g$. The subsequent increase in γ due to acceleration does not affect the emittance since this process is slow on the betatron time scale. However, the emittance begins to increase again when electrons advance into the tail of the laser pulse and $d\epsilon_{nx}^2/dt = a_0[\langle x_0\dot{x}_0\rangle\langle x_0\delta\rangle - \langle x_0^2\rangle\langle\dot{x}_0\delta\rangle]/\gamma^2$ where $\delta = 1 - v_z/v_p = 1/2\gamma_z^2 + 1/2\gamma_g^2$ and v_p and a_0 are the phase velocity and amplitude of the laser, respectively, at the point of interaction. The final emittance of the electron bunch scales with the transverse cross section originally occupied by these electrons. As the bubble initially forms, plasma electrons close to the axis, $r_0 (\approx 1\ \mu\text{m}) \ll r_{\max}$, can stream through the laser pulse, while those situated where the ponderomotive force is largest, at a distance from the axis of the order of $r_{\max} = w_0/2$, are deflected to form the sheath of the bubble at radius $R = 2\sqrt{a_0}c/\omega_p$. For our parameter range, $a_0 \leq 3$, $r_{\max} \approx 5\ \mu$m and $R = 5.5\ \mu$m. PIC simulations using OSIRIS confirm that electrons within a radius $r \leq r_0 = r_{\max}/4$ can initially stream through and become trapped. The capture cross section shape and area depends on the buildup of sheath electrons at the crossing point situated at the rear of the bubble. The actual distribution depends on the bubble parameters, which in turn depend on the laser pulse shape and intensity, plasma density, etc. However, electrons streaming back through the bubble are injected to form the nascent bunch, which then deflects incoming electrons close to the axis, $r \leq r_0$, and causes beam loading thus distorting the global potential inside the bubble [28]. The combined effect of deflection and beam loading shuts off injection above a particular current density. The resulting bunch of captured electrons is contained in a small volume $\delta V = \sigma_z\sigma_r^2$, with width σ_r and length σ_z; the latter may depend on the bunch charge, Q, due to its role in shutting off injection. The final transverse emittance therefore scales with Q/σ_z. As the emittance is proportional to $r\theta$, the product of bunch radius and divergence angle, we find that $\theta \propto Q^{1/2}\sigma_z^{-1/2}$. The brightness $B = I/4\pi^2\epsilon_{nx}\epsilon_{ny}$, is inversely proportional to σ_z and proportional to Q, when emittance growth due to resonant driven betatron motion is negligible. Figure 5

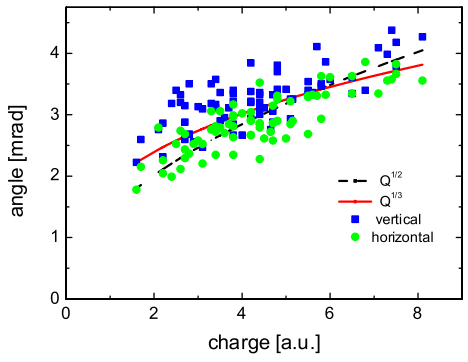

FIG. 5 (color online). Beam divergence measured as a function of bunch charge in vertical and horizontal planes. Lines show scaling with $Q^{1/2}$ and $Q^{1/3}$, respectively.

shows the measured beam divergence plotted as a function of Q for bunch charges up to about 10 pC. This follows a $\theta \propto Q^{1/2}\sigma_z^{-1/2}$ dependence within experimental error for the cases where σ_z is constant ($Q^{1/2}$ scaling) and where $\sigma_z \propto Q^{1/3}$ ($Q^{1/3}$ scaling for uniform increase of σ_z with Q). These measurements imply that the injected bunch length either remains constant (≈ 1 fs in our case) with increase in Q or only increases very slowly. The case of σ_r constant (which gives a constant θ) is highly unlikely because of the measured θ dependence on charge. The spread in angles is most likely due to variation of the betatron orbit radius, which fluctuates between extrema, as shown in Fig. 4(c).

The subsequent propagation of the bunches along the beam line has been simulated using General Particle Tracer (GPT) [29], showing that space charge induces an emittance growth of up to 50% after 1 m for charges of the order of 1–10 pC for an electron energy of 100 MeV. It is therefore likely that electron beams with emittance as low as 0.3–0.4π mm mrad have been produced, which is beyond the resolution limit of our detection system.

In conclusion, we report single-shot, high-resolution emittance measurements of laser-accelerated electron beams. We show measurements of the horizontal and vertical emittance that set an upper limit of $\epsilon_{nx} = 2.2 \pm 0.7\pi$ mm mrad and $\epsilon_{ny} = 2.3 \pm 0.6\pi$ mm mrad (average values), respectively, for an electron energy of 125 ± 3 MeV. The error in measurement of the spot size ≈ 1 μm gives an error of about 0.5π mm mrad. The measured emittance is consistent with a 1 fs electron bunch. Because of the short bunch length, the peak currents are as high as 10 kA. The peak transverse beam brightness is thus estimated as $B = I/4\pi^2\epsilon_{nx}\epsilon_{ny} \approx 5 \times 10^{15}$ A m^{-1} rad^{-1}. If coupled to an undulator, such beams should produce coherent UV radiation in a FEL with a peak brilliance in excess of 10^{22} photons/(s mrad^2 mm^2 0.1% bandwidth) [19]. With further acceleration using a higher power laser it may be possible to construct a table top x-ray FEL, thereby transforming the use of coherent light sources at short wavelengths.

*d.a.jaroszynski@strath.ac.uk

[1] P. O'Shea and H. Freund, Science **292**, 1853 (2001).
[2] D. Bilderback, P. Elleaume, and E. Weckert, J. Phys. B **38**, S773 (2005).
[3] H. Wiedemann, *Particle Accelerator Physics* (Springer, New York, 2007).
[4] S. Khan, J. Mod. Opt. **55**, 3469 (2008).
[5] E. Esarey, C. B. Schroeder, and W. P. Leemans, Rev. Mod. Phys. **81**, 1229 (2009).
[6] T. Tajima and J. M. Dawson, Phys. Rev. Lett. **43**, 267 (1979).
[7] S. Mangles *et al.*, Nature (London) **431**, 535 (2004).
[8] C. Geddes *et al.*, Nature (London) **431**, 538 (2004).
[9] J. Faure *et al.*, Nature (London) **431**, 541 (2004).
[10] W. P. Leemans *et al.*, Nature Phys. **2**, 696 (2006).
[11] H. P. Schlenvoigt *et al.*, Nature Phys. **4**, 130 (2008).
[12] M. Fuchs *et al.*, Nature Phys. **5**, 826 (2009).
[13] J. G. Gallacher *et al.*, Phys. Plasmas **16**, 093102 (2009).
[14] S. Wiggins (to be published).
[15] S. Humphries, *Charged Particle Beams* (Wiley, New York, 1990).
[16] K. McDonald and D. Russell, in *Frontiers of Particle Beams.* (Springer, Berlin, 1989) p. 122.
[17] Y. Yamazaki, T. Kurihara, H. Kobayashi, I. Sato, and A. Asami, Nucl. Instrum. Methods Phys. Res., Sect. A **322**, 139 (1992).
[18] S. Fritzler *et al.*, Phys. Rev. Lett. **92**, 165006 (2004).
[19] C. M. S. Sears *et al.*, Phys. Rev. ST Accel. Beams **13**, 092803 (2010).
[20] N. Delerue *et al.*, in *Proceedings of the 23rd Particle Accelerator Conference, Vancouver, Canada* (IEEE, Piscataway, NJ, 2009).
[21] D. Jaroszynski *et al.*, Phil. Trans. R. Soc. A **364**, 689 (2006).
[22] G. A. Mourou, T. Tajima, and S. V. Bulanov, Rev. Mod. Phys. **78**, 309 (2006).
[23] W. Lu *et al.*, Phys. Rev. ST Accel. Beams **10**, 061301 (2007).
[24] S. Agostinelli *et al.*, Nucl. Instrum. Methods **506**, 250 (2003).
[25] M. Zhang, Tech. Rep. No. FERMILAB-TM-1988, 1996.
[26] R. Fonseca and others, in *Proceedings of Computational Science-ICCS 2002, Pt III*, Lecture Notes in Computer Science Vol. 2331 (Springer, Berlin/Heidelberg, 2002), pp. 342–351.
[27] K. Nemeth *et al.*, Phys. Rev. Lett. **100**, 095002 (2008).
[28] C. Rechatin *et al.*, New J. Phys. **12**, 045023 (2010).
[29] S. van der Geer *et al.*, in *Computational Accelerator Physics 2002* Vol. 175 (Institute of Physics, Bristol, UK, 2005), p 101.